Alzheimer's Research & Therapy

RESEARCH

Open Access

CT-derived brain volumes and plasma p-Tau217 for risk stratification of amyloid positivity in early-stage Alzheimer's disease

Sohyun Yim[1†], Seongbeom Park[2†], Kyoung Yoon Lim[2], Heekyoung Kang[1], Daeun Shin[1], Hyemin Jang[3], Michael Weiner[4], Henrik Zetterberg[5,6,7,8,9,10], Kaj Blennow[5,6,11,12], Fernando Gonzalez-Ortiz[5,6], Nicholas J. Ashton[5,13,14,15], Sung Hoon Kang[16], Jihwan Yun[17], Minyoung Chun[18,19], Eunjoo Kim[20], Heejin Kim[1,21,22,23], Duk L. Na[1,21], Jun Pyo Kim[1,21], Sang Won Seo[1,21,22,23*†], Kichang Kwak[2*†] and K-ROAD study

Abstract

Background Early detection of amyloid-β (Aβ) pathology is critical for timely intervention in Alzheimer's disease (AD). While Aβ positron emission tomography (PET) and cerebrospinal fluid (CSF) biomarkers are accurate, their high cost and limited accessibility hinder routine use. We developed a computed tomography (CT)-based, two-stage workflow combining CT-derived atrophy patterns with plasma phosphorylated tau 217 (p-Tau217) to predict Aβ PET positivity.

Methods In this cohort of 616 participants (521 with mild cognitive impairment (MCI], 95 with early dementia of Alzheimer's type (DAT]; age 60–93 years), CT, p-Tau217 assays, and Aβ PET were performed. A random forest model incorporating CT-derived regional W-scores and apolipoprotein E ε4 (APOE ε4) status stratified individuals into low-, intermediate-, and high-risk groups. p-Tau217 testing was reserved for the intermediate-risk group.

Results At a 95% sensitivity/specificity threshold, CT-based stratification yielded a low-risk negative predictive value (NPV) of 95.8% (93.0–98.6%) and a high-risk positive predictive value (PPV) of 98.4% (96.8–100.0%), with 28.2% classified as intermediate-risk. Targeted plasma testing of intermediate-risk group improved the overall PPV to 92.8% (88.5–97.1%) and the overall NPV to 88.9% (78.6–99.2%), achieving an overall accuracy of 95.8% (94.2–97.4%). The CT-based workflow's accuracy was non-inferior to our MRI-based method (area under the curve 0.96 vs. 0.95; $p = 0.14$).

Conclusions This CT-based, two-stage approach is a cost-effective, scalable alternative to MRI-based strategies, leveraging routine CT and selective p-Tau217 testing to enhance early AD detection and optimize resource utilization in clinical practice.

Keywords Alzheimer's disease, Two-stage diagnostic workflow, Amyloid status, Computed tomography, Plasma p-tau217, Machine learning

†Sohyun Yim and Seongbeom Park contributed equally to this article as co-first authors.

†Sang Won Seo and Kichang Kwak contributed equally to this article as co-corresponding authors.

*Correspondence:
Sang Won Seo
sw72.seo@samsung.com
Kichang Kwak
kichang.kwak@beaubrain.bio
Full list of author information is available at the end of the article

Background

Alzheimer's disease (AD) is characterized by extracellular amyloid-β (Aβ) plaques and intracellular tau neurofibrillary tangles, leading to progressive neurodegeneration [1–3]. Recent advancements in Aβ-targeted therapies highlight the critical importance of timely detection of Aβ pathology, particularly in patients with mild cognitive impairment (MCI) or early dementia of Alzheimer's-type (DAT) [4–6]. Aβ positron emission tomography (PET) remains the only in vivo gold standard for detecting Aβ deposition [7–9] and is increasingly available at specialized centers; however, its high cost and reliance on cyclotron-produced tracers limit broad clinical deployment [10]. Cerebrospinal fluid (CSF) biomarkers provide valuable supportive information [11–13] but are not considered standalone gold standards due to their invasiveness and inter-laboratory variability [14]. Plasma biomarkers such as phosphorylated tau 217 (p-tau217) have emerged as minimally invasive alternatives [15–18], but their additional expense limits their practicality for routine screening.

Structural imaging, including magnetic resonance imaging (MRI) and computed tomography (CT), is routinely performed in initial clinical assessments of cognitive impairment to rule out potentially reversible conditions, such as brain tumors, subdural hematomas, or strokes, thus incurring no additional costs [19, 20]. AD typically manifests as characteristic regional atrophy patterns, including medial temporal and posterior parietal regions, observed as sulcal widening and ventricular enlargement [21–24]. Leveraging these distinctive patterns, structural imaging can efficiently stratify patients into low-risk and high-risk groups for Aβ pathology, reducing unnecessary biomarker tests.

Previously, we introduced a two-stage diagnostic workflow combining MRI-derived brain atrophy measures with plasma p-tau217 testing, effectively identifying Aβ-positive patients while optimizing resource utilization [25]. However, MRI has significant limitations, such as relatively high costs, prolonged scan durations, and contraindications (e.g., claustrophobia or metallic implants) [26–28]. Conversely, CT is more accessible, cost-effective, and widely used clinically, particularly in initial dementia assessments where MRI may be unavailable, contraindicated, or impractical. In many real-world healthcare settings, especially in Europe, CT serves as the first-line imaging modality due to its rapid acquisition and lower cost. Although CT's limited resolution previously necessitated subjective visual ratings prone to variability, recent advances in artificial intelligence, particularly deep learning-based segmentation, now enable precise and objective quantification of brain atrophy [29]. We previously validated a CT-based artificial intelligence (AI) framework against MRI, demonstrating reliable, region-specific atrophy measures and accurate differentiation of cognitive stages and dementia subtypes. A brief description of this work is provided in eNote 1. The technical implementation of the CT-based model used in this study, including the W-score derivation, is described in a previously published validation study [30].

Building upon these developments, this study aims to validate a clinically feasible two-stage, consisting of 1) AI-supported classification of individuals into low-, intermediate-, and high-risk of amyloid positivity; and 2) selective p-tau217 testing exclusively for the intermediate-risk group. We hypothesized that this CT-based workflow would achieve diagnostic accuracy comparable to the MRI-based approach, substantially improving clinical accessibility, economic efficiency, and scalability for broader real-world implementation.

Methods

Participants

A total of 616 participants (521 with MCI and 95 with early-stage DAT), aged 60 to 93 years, were recruited from the Korea-Registries to Overcome Dementia and Accelerate Dementia Research (K-ROAD) project in South Korea [31]. A detailed participant selection process is illustrated in eFigure 1. Participants with MCI were diagnosed based on Petersen's clinical criteria for amnestic MCI with the following modifications [32, 33]: subjective memory complaints reported by the patient or caregiver, no significant impairment in activities of daily living (ADL), objective cognitive decline below −1.0 standard deviation (SD) of age- and education-matched norms in neuropsychological tests, and not being demented. Diagnosis of early-stage DAT was established according to the 2011 criteria from the National Institute on Aging and Alzheimer's Association [34], with a Clinical Dementia Rating (CDR) score of 0.5.

All participants underwent a comprehensive dementia evaluation, including clinical interviews, neurological examinations, and standardized neuropsychological assessments using the Seoul Neuropsychological Screening Battery (SNSB) [35]. Further assessments included routine blood tests to exclude medical conditions (vitamin B12 deficiency, syphilis serology, thyroid, renal, or hepatic dysfunction), structural brain imaging to identify lesions such as territorial infarction, intracranial hemorrhage, brain tumors, or severe white matter hyperintensities based on the modified Fazekas ischemic scale [36], apolipoprotein E (APOE) genotyping, and Aβ PET-CT imaging. Participants with cognitive impairment due to these secondary causes or other neurodegenerative diseases (progressive supranuclear palsy, corticobasal

syndrome, frontotemporal dementia, or Lewy body/Parkinson's disease dementias) were excluded.

Aβ PET acquisition and determination of Aβ positivity

All participants underwent Aβ PET using either [^{18}F] florbetaben (FBB) or [^{18}F]flutemetamol (FMM) to detect amyloid in the brain. Following protocols recommended by the ligand manufactures, a 20 min emission PET scan with dynamic mode (consisting of 4 × 5 min frames) was performed 90 min after the injection of a mean dose of 311.5 MBq FBB and 185 MBq FMM, respectively.

PET scans were aligned with the participants' MRI images and normalized to the Montreal Neurological Institute-152 standard using the appropriate transformation matrix. Following alignment, the gray matter of the brain was divided into 116 regions based on the automated anatomical labeling atlas. The entire cerebellum served as the reference region for calculating the standardized uptake value ratio (SUVR), with regional masks obtained from the Global Alzheimer's Association Interactive Network (GAAIN) website (https://www.gaain.org/). We assessed Aβ burden in FBB and FMM PET scans using the BeauBrain Amylo software, which employs image processing methodologies based on the Centiloid (CL) project [37]. Aβ PET positivity was defined using a threshold of 20 CL, which was selected to enhance sensitivity for early Aβ detection, based on prior studies that validated the use of a lower CL cutoff in preclinical and at-risk populations [38–40].

Plasma collection and processing for p-Tau217 analysis

Blood samples were collected from each participant, placed into 0.5M EDTA-containing tubes, and mixed for 5 min. The samples were centrifuged at 1,300 g for 10 min, after which plasma was extracted and aliquoted into 5 or 10 vials, each containing 0.3 mL. These plasma samples were stored at − 75 °C following the guidelines established by the National Biobank of the Republic of Korea for human resource collection and registration. The frozen plasma samples were then shipped at − 70 °C to the Department of Psychiatry and Neurochemistry at the University of Gothenburg, where plasma concentrations of p-Tau217 were measured using the commercial ALZpath p-Tau217 immunoassay on the Single Molecule Array (SIMOA) HD-X instrument, a paramagnetic microbead-based sandwich enzyme-linked immunosorbent assay system (Quanterix, Billerica, MA).

Image acquisition and preprocessing

CT imaging was performed using a Discovery STe PET-CT scanner (GE Medical Systems, Milwaukee, WI, USA), operating in three-dimensional mode and acquiring 47 slices, each 3.3-mm thick, covering the entire brain. Additional CT images for attenuation correction were obtained using a 16-slice helical CT (140 keV, 80 mA, 3.75-mm section width) and reconstructed in a 512 × 512 matrix. Voxel size of the PET-CT acquired CT images was 0.5 mm × 0.5 mm × 3.27 mm. Signal-to-noise ratio validation was conducted through a phantom study (120 kVp, 190 mA, 3.75 mm slice thickness). The CT images underwent standardization to normalize brain tissue Hounsfield units (HU), following previously validated methods [41]. Subsequently, standardized CT images were co-registered to the corresponding T1-weighted MRI images using Advanced Normalization Tools (ANTs) [42].

AI-driven CT-based brain atrophy assessment

We performed an AI-powered CT analysis using BeauBrain Morph Software [29], which provides quantitative brain atrophy measurements from noncontrast CT scans. This fully automated approach delineates 14 anatomically defined regions—including bilateral cerebrospinal fluid spaces in the frontal, occipital, parietal, and temporal lobes and ventricular segments (anterior lateral, posterior, temporal horns)—and generates W-scores, which are standardized residual derived from linear regression model that adjust individual regional brain volumes for age and sex [43]. These scores quantify the degree to which an individual's volume deviates from the expected norm, based on a large, normative reference groups from the K-ROAD cohort (n = 1200; age 24–89 years; 60.7% female).

Development of a CT-based two-stage workflow for Aβ positivity prediction

The model incorporated APOE genotype and CT-derived brain volumes to stratify the risk of Aβ PET positivity. Specifically, a binary random forest classifier was trained using APOE ε4 carrier status and CT-derived regional brain volume W-scores as predictors, with PET positivity defined as a CL value ≥ 20. The classifier first predicted each participant's probability of being amyloid positive. These predicted probabilities from this classifier were then used to stratify participants into three risk groups: low-, intermediate-, and high-risk groups. To achieve this, two probability thresholds were defined for each threshold strategy (90%, 95%, and 97.5%): a Lower threshold to achieve the target sensitivity to reduce false negatives, and an upper threshold to achieve the target specificity to reduce false positives. Participants with predicted probabilities below the Lower threshold were classified as low risk, those above the upper threshold as high risk, and those between the two thresholds as intermediate risk. For example, under the 95%/95% threshold strategy, thresholds for 95% sensitivity and 95% specificity

were derived from the pooled MCI and DAT cohort and then applied to each subgroup to confirm consistent stratification performance. We then calculated the prevalence of Aβ PET negativity in the low-risk group and positivity in the high-risk group for each threshold strategy. In the second stage, plasma p-Tau217 testing was applied exclusively to participants in the intermediate-risk group. Using a previously established threshold for p-Tau217 positivity [44], we assessed concordance with Aβ PET status to refine Aβ positivity predictions. Overall diagnostic accuracy was defined as the proportion of correctly classified cases, and workflow efficiency was measured by the reduction in the number of participants requiring additional biomarker testing.

MRI acquisition and processing for comparative analysis

For comparison with the CT-based two-stage diagnostic workflow, MRI scans were acquired in the same participant cohort using a 3.0 T MRI scanner (Philips 3.0 T Achieva) and a 3D T1 turbo field-echo sequence (1.0 mm sagittal slices with 50% overlap; TR 9.9 ms; TE 4.6 ms; flip angle 8°; reconstructed matrix 480×480 pixels; field of view 240 mm). CT and MRI exams were performed within a median interval of 2.6 months (IQR 0.9–4.7 months). Using methods previously described in detail [30], MRI images underwent quantitative brain atrophy measurements targeting the same 14 regions of interest (ROIs) as used in the CT analysis, generating age- and sex-adjusted regional W-scores. Furthermore, as previously detailed [45], a two-stage workflow integrating MRI-derived W-scores with plasma p-Tau217 was conducted to directly evaluate the comparative performance relative to the CT-based approach.

Statistical analysis

All statistical analyses were conducted using R software (version 4.0.2; http://www.r-project.org). Descriptive statistics were computed to summarize demographic and clinical characteristics of the study population. Group differences in continuous variables were assessed using analysis of variance (ANOVA), with Tukey's post hoc tests applied where appropriate. Categorical variables were compared using chi-square tests, and Bonferroni correction was employed for multiple pairwise comparisons as needed.

For the classifier development described above, predictive modeling was performed in Python (version 3.8) using the scikit-learn (https://scikit-learn.org/stable/index.html) library for machine learning. The primary predictive features included APOE ε4 carrier status and CT-derived regional W-scores, which were selected based on their known associations with Aβ pathology. Model performance was evaluated through *k*-fold cross-validation (with $k=5$) and quantified using accuracy, positive predictive value (PPV), and negative predictive value (NPV) metrics. For each fold in the cross validation procedure, the model was trained on a subset of the data (training set) and evaluated on the corresponding held-out test set. This process was repeated across all five folds to assess predictive performance. Hyperparameter optimization was conducted via grid search with internal cross-validation applied within each training fold to ensure test fold remained unseen during model selection. Key parameters of the random forest model were tuned, including *n_estimators, max_depth, min_samples_split, min_samples_leaf, and max_features*. The same modeling pipeline was applied consistently across all iterations to ensure robustness and reproducibility.

Risk stratification thresholds were established based on target sensitivity and specificity levels (90%, 95%, and 97.5%), and were used to classify participants into low-, intermediate-, and high-risk groups. For individuals in the intermediate-risk group, plasma p-Tau217 data were incorporated to refine Aβ PET status predictions, and the concordance between plasma biomarker results and Aβ PET status was evaluated. The McNemar's test was used to compare accuracy, sensitivity, and specificity, while PPV and NPV were compared using a bootstrapping-based test. The statistical significance was evaluated using a two-tailed test with an alpha level of 0.05.

Results

Participant characteristics

The demographics of participants are presented in Table 1. A total of 616 participants were included in the study. The median age was 73.0 years, with 60.6% female and 47.0% *APOE ε4* carriers. The median plasma p-Tau217 concentration was 0.7 pg/mL (IQR 0.3–1.1 pg/mL). Aβ PET positivity was observed in 63.9% of participants, and the median CDR-SOB score was 1.5.

Primary risk stratification via CT-based brain atrophy patterns

In the first stage, CT-based atrophy measures stratified participants into low-, intermediate-, and high-risk groups for Aβ PET positivity (Fig. 1A). At sensitivity/specificity thresholds of 90%, 95%, and 97.5%, the CT model achieved NPVs of 94.9%, 95.8%, and 96.4% (low-risk) and PPVs of 97.6%, 98.4%, and 99.1% (high-risk), with 21.3%, 28.2%, and 36.5% of participants in the intermediate-risk group, respectively. Detailed demographics at this threshold are provided in supplementary material (eTable 1). We selected the 95% threshold as optimal, balancing predictive accuracy and Limiting the intermediate-risk cohort to 28.2%, thereby minimizing downstream

Table 1 Demographics of study participants

	Participants ($n=616$)
Diagnosis, MCI *n* (%)	521 (84.6)
Age, years	73.0 (68.0–78.0)
Sex, female *n* (%)	373 (60.6)
Education, years	12.0 (8.0–16.0)
APOE ε4 carriers, *n* (%)	289 (46.9)
Aβ PET positive, *n* (%)	393 (63.8)
Plasma p-Tau217, pg/ml *	0.7 (0.3–1.1)
CDR-SOB	1.5 (1.0–3.0)
Median interval between CT and MRI scans, months	2.6 (0.9–4.7)

Data are presented as *n* (%) for categorical variables and median with interquartile range (IQR) for continuous variables. Abbreviations: MCI, mild cognitive impairment; APOE, apolipoprotein E; Aβ PET, amyloid-beta positron emission tomography; p-Tau217, phosphorylated tau 217; CDR-SOB, clinical dementia rating–sum of boxes; CT, computed tomography; MRI, magnetic resonance imaging

testing costs (Fig. 2). At this threshold, 74.8% of MCI participants in the intermediate-risk group and 98.0% in the high-risk group were Aβ PET positive, while only 3.3% of those in the low-risk group were positive. Among DAT participants, 94.9% in the intermediate-risk group and 100% in the high-risk group were Aβ PET positive, compared to 22.2% in the low-risk group (Table 2).

As a supportive comparator, an MRI-based model produced comparable performance (NPV 98.2%, PPV 98.3%, 34.3% intermediate-risk at 95% threshold; Fig. 1B), with no statistically significant differences (AUC: $p=0.14$, NPV: $p=0.82$, and PPV: $p=0.57$) when compared to the CT-based model, thereby confirming that CT-based stratification alone offers robust predictive power with the advantage of greater accessibility and lower cost.

Refining Aβ PET status with p-Tau217 in CT-identified intermediate-risk participants

In the second stage of our CT-first workflow, plasma p-Tau217 testing was applied only to the 28.2% of participants in the CT-based intermediate-risk group (Fig. 3A). At the 95% sensitivity/specificity threshold, this yielded a PPV of 96.9% and NPV of 74.7%, within the intermediate-risk group. Across the entire cohort, targeted plasma testing of the intermediate-risk group improved the overall PPV to 92.8% (95% CI: 88.5–97.1%) and the overall NPV to 88.9% (95% CI: 78.6–99.2%), boosting overall two-stage accuracy to 95.8% (95% CI: 94.2–97.4%) and reducing further biomarker testing by 71.8%. The one-step CT-only model achieved an AUC of 0.81 for predicting amyloid positivity. Incorporating plasma p-Tau217 (two-step CT + p-Tau217) increased the AUC to 0.96 (DeLong's test, $p<0.001$; Fig. 4A) and significantly improved PPV and NPV within the CT intermediate subgroup (McNemar's test, $p<0.01$; Fig. 4C).

For comparison, plasma p-Tau217 applied to the 34.3% MRI-based intermediate group (Fig. 3B) yielded a PPV of 96.3%, an NPV of 70.6%, and an overall two-stage accuracy of 95.2%. The one-step MRI-only model had an AUC of 0.81, which rose to 0.95 with the addition of plasma p-Tau217 ($p<0.001$; Fig. 4B).

Discussion

In this study, we developed and validated a two-stage diagnostic workflow integrating CT-derived brain atrophy patterns and plasma p-Tau217 testing to predict Aβ PET positivity in individuals with MCI or mild dementia. Our major findings were as follows: First, CT-based

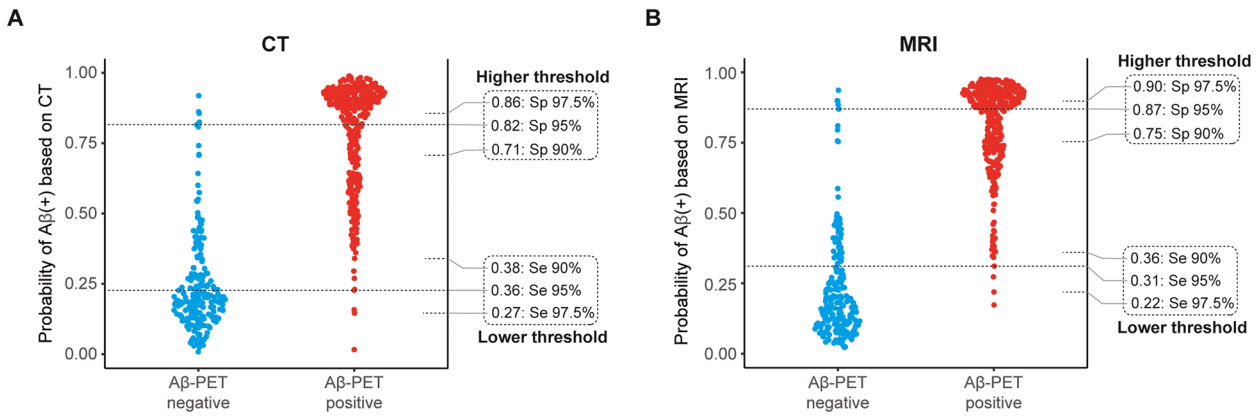

Fig. 1 Distribution and thresholds of Aβ (+) probability based on brain atrophy patterns in the K-ROAD cohort. Predictions based on CT-derived **A** and MRI-derived **B** brain atrophy patterns. Blue dots represent Aβ PET negative individuals, and red dots represent Aβ PET positive individuals. The right *y*-axis shows predicted probabilities of Aβ probability, with thresholds corresponding to sensitivity(Se) and specificity(Sp) levels of 90%, 95%, and 97.5%. These thresholds define the boundaries for low-, intermediate-, and high-risk groups. Abbreviations: Aβ, amyloid-beta; PET, positron emission tomography; CT, computed tomography; MRI, magnetic resonance imaging; Se, sensitivity; Sp, specificity

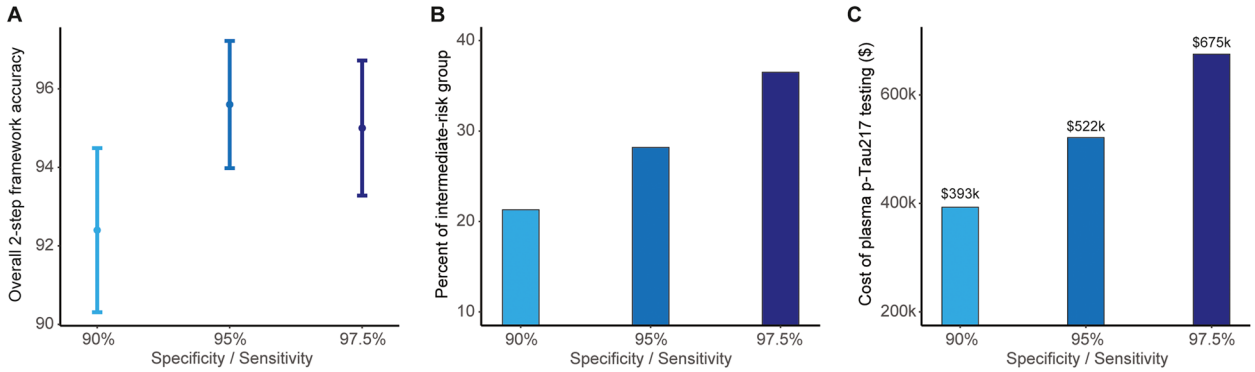

Fig. 2 Workflow performance and cost evaluation based on risk stratification thresholds. **A** Overall accuracy of the CT-based two-step classification workflow, including accuracy within the low- and high-risk groups, as well as the classification accuracy using plasma p-Tau217 in the intermediate-risk group. Error bars represent 95% confidence intervals. **B** Proportion of individuals assigned to the intermediate-risk group under different risk threshold strategies. **C** Estimated total cost for each strategy, incorporating the added expense of plasma p-Tau217 testing for individuals in the intermediate-risk group. Abbreviations: p-Tau217, phosphorylated tau 217

Table 2 Risk stratification for A β PET positivity using different threshold strategies across cognitive staging

K-ROAD			
Risk groups	**Participants in risk group, n (%)**	**Cognitive status**	
		A β PET positive MCI, n (%)	**A β PET positive DAT, n (%)**
90% Se Lower-risk threshold/90% Sp higher-risk threshold			
Low risk	195 (31.7%)	186 (4.3%)	9 (22.2%)
Intermediate risk	131 (21.3%)	104 (72.1%)	27 (92.6%)
High risk	290 (47.1%)	231 (97.0%)	59 (100%)
95% Se Lower-risk threshold/95% Sp higher-risk threshold			
Low risk	191 (31.0%)	182 (3.3%)	9 (22.2%)
Intermediate risk	174 (28.2%)	135 (74.8%)	39 (94.9%)
High risk	251 (40.7%)	204 (98.0%)	47 (100%)
97.5% Se Lower-risk threshold/97.5% Sp higher-risk threshold			
Low risk	167 (16.9%)	159 (3.1%)	8 (12.5%)
Intermediate risk	377 (46.7%)	176 (67.0%)	49 (95.9%)
High risk	224 (36.4%)	186 (98.9%)	38 (100%)

Data are presented as n or n (%). The first column indicates each of the evaluated strategies for CT-based risk stratification, along with the corresponding low-, intermediate- and high-risk groups for each strategy. The second column shows the number of screened individuals assigned to each risk category, with the percentage in the intermediate-risk group presented in parentheses. The third and fourth columns present the Aβ PET positivity rates within each risk group, stratified by cognitive stage

Abbreviations: *Aβ* Amyloid-β, *K-ROAD* Korean Brain Aging Study for the Early Diagnosis and Prediction of Alzheimer's Disease, *Se* Sensitivity, *Sp* Specificity

stratification accurately differentiated low-, intermediate-, and high-risk groups for amyloid positivity, achieving predictive values comparable to previously validated MRI-based approaches. Second, targeted plasma p-Tau217 testing significantly refined diagnostic accuracy within the intermediate-risk group, resulting in high PPV and clinically acceptable NPV. Finally, the proposed CT-based workflow demonstrated high overall accuracy (95.8%) while substantially reducing the number of participants requiring additional invasive biomarker testing. Collectively, these results highlight the clinical feasibility, practicality, and scalability of CT-based two-stage strategies for amyloid risk assessment.

Our first major finding demonstrated that CT-based regional atrophy measures reliably stratified Aβ PET positivity risk into clearly defined risk groups. At the optimal threshold (95% sensitivity/specificity), the CT-based stratification achieved PPVs of 98.4% in the high-risk group and NPVs of 95.8% in the low-risk group, closely matching the performance of previously validated

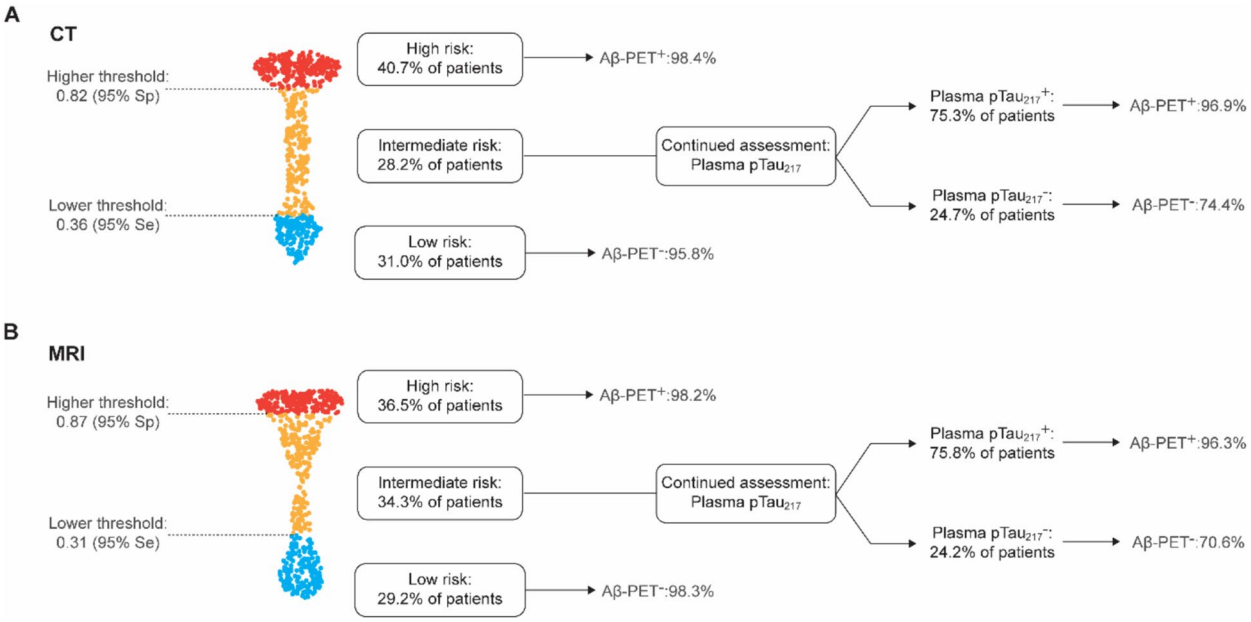

Fig. 3 Two-stage diagnostic workflow for predicting Aβ positivity on PET using CT-based (**A**) and MRI-based (**B**) risk stratification followed by plasma p-Tau217 testing. The panel **A** and **B** illustrate two-stage diagnostic workflows based on the 95% sensitivity and 95% specificity threshold strategies. The left side of each panel shows the initial risk stratification using CT and MRI, with individuals categorized into high (red), intermediate (yellow), and low (blue) risk groups. The percentage of Aβ PET positive individuals in the high-risk group and the percentage of Aβ PET negative individuals in the low-risk group reflects the predictive accuracy of the first step. The right side presents the second step, plasma p-Tau217 testing applied only to the intermediate-risk group. Predictive accuracy in this step is indicated by the negative predictive value and positive predictive value. Abbreviations: Aβ, amyloid-beta; PET, positron emission tomography; CT, computed tomography; MRI, magnetic resonance imaging; p-Tau217, phosphorylated tau 217; Se, sensitivity; Sp, specificity

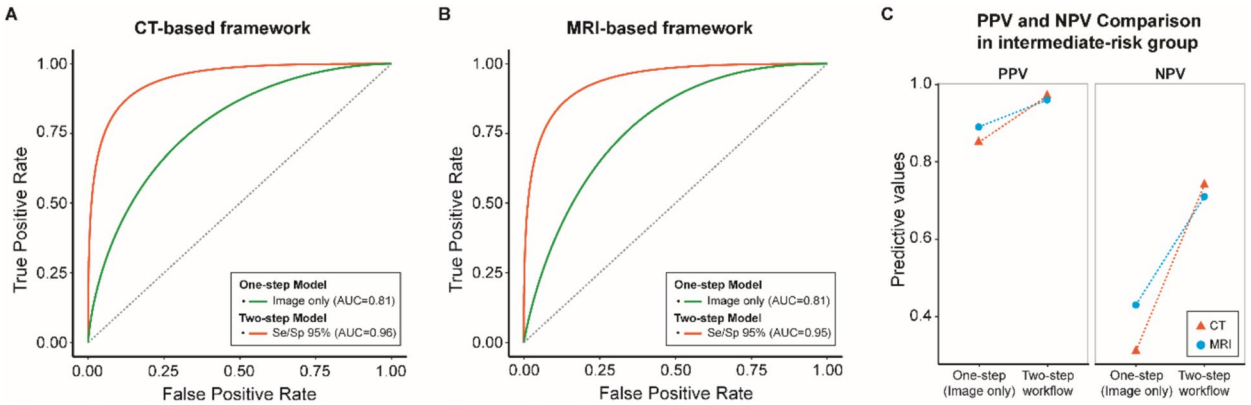

Fig. 4 Model performance and predictive value across modality. Receiver operating characteristic curves for the CT-based **A** and MRI-based framework **B**, comparing the performance of the one-step (image-only) model and the proposed two-step model. **C** Comparison of PPV and NPV between the one-step and two-step models within the intermediate-risk groups across modality. Abbreviations: AUC, area under the curve; CT, computed tomography; MRI, magnetic resonance imaging; NPV, negative predictive value; PPV, positive predictive value; Se, sensitivity; Sp, specificity

MRI-based methods. These findings are consistent with prior studies emphasizing characteristic atrophy patterns in AD, particularly in the medial temporal and posterior parietal regions. Leveraging routinely performed CT scans, our approach offers significant practical advantages by avoiding additional costs, making it particularly suitable for widespread clinical adoption, especially in resource-limited settings.

Our second major finding highlighted the added value of plasma p-Tau217 testing in refining amyloid

status prediction for the intermediate-risk group. Plasma p-Tau217 testing achieved a high PPV (96.9%) and acceptable NPV (74.7%), comparable to results from MRI-based approaches. This confirms previous evidence that plasma p-Tau217 effectively complements structural imaging data, providing robust biochemical confirmation of amyloid pathology. By selectively employing plasma biomarkers for uncertain cases, our two-stage workflow significantly enhances diagnostic precision while optimizing resource use and balancing accuracy with economic practicality.

Our final major finding was the substantial clinical utility and resource-saving potential of the CT-based two-stage workflow. Using this approach, we achieved an overall accuracy of 95.8%, comparable to previously validated MRI-based workflows, while notably reducing the need for additional invasive testing by approximately 72%. Unlike MRI, which can be costly, time-consuming, and contraindicated in certain patient groups, CT imaging is faster, more affordable, and broadly accessible. Employing advanced AI-based segmentation techniques, our CT-based workflow addresses critical Limitations of MRI and PET, making it practical for broader clinical implementation and capable of extending early amyloid detection beyond specialized centers into community-based practice. To contextualize the economic implications of our approach, we estimated the cost of identifying 1,000 Aβ-positive individuals. Under a universal PET strategy, approximately 1,567 individuals would require scanning at a total cost of USD 6.27 million (assuming USD 4,000 per scan; 63.8% Aβ positivity rate). In contrast, our two-stage workflow restricts plasma biomarker testing to the intermediate-risk group, comprising 28.2% of participants, resulting in an estimated cost of USD 132,600 (assuming USD 300 per plasma test) and a total cost reduction exceeding USD 6.1 million.

A major strength of our study is the validation of a clinically feasible, AI-driven CT segmentation framework, offering precise and objective regional atrophy measures comparable to MRI-based assessments. However, there are several limitations. First, although our CT-first two-stage workflow markedly enhanced diagnostic accuracy over a CT-only baseline, the incremental gain was modest, which may temper its clinical impact; nonetheless, even small improvements in amyloid detection can meaningfully guide patient management and therapeutic decisions. Second, regional atrophy patterns—while characteristic of AD—are not wholly specific and can occur in other disorders (e.g., Limbic-predominant age-related TAR DNA-binding protein 43 encephalopathy or hippocampal sclerosis), underscoring the need for multimodal confirmation. Third, our model disproportionately allocated APOE ε4 carriers to the high-risk group (eTable 1), suggesting potential over-weighting of this variable (eFigure 2). While the 73.5% ε4 carrier frequency among amyloid-positive individuals in our cohort aligns with prior reports [46], future refinements should incorporate feature regularization and external validation to enhance generalizability. Finally, because our cohort was drawn from a specialized memory clinic, the workflow may not directly generalizable to settings such as prevention trials, where neuroimaging is not routinely performed. In addition, since the cutoff value was determined using the assessed cohort, the study may not include a truly independent dataset to evaluate the full pipeline, which could somewhat limit the generalizability of the findings. However, in patients with MCI or mild dementia, the use of structural imaging remains clinically justified. Future studies in broader, community-based populations will be essential to establish generalizability. Nonetheless, given the substantial practical advantages of our CT-based two-stage diagnostic workflow—high accuracy, cost-effectiveness, and broad clinical accessibility—our findings hold significant potential for improving early and precise diagnosis in real-world clinical settings.

Conclusion

In conclusion, our CT-based two-stage diagnostic workflow effectively predicts amyloid PET positivity in patients with MCI and early dementia, demonstrating diagnostic accuracy comparable to previously validated MRI-based workflows while substantially enhancing clinical accessibility, efficiency and scalability. Given its practicality and potential for broad clinical implementation, this CT-based approach offers a highly promising strategy to facilitate early and accurate diagnosis, optimize patient selection for amyloid-targeted therapies, and improve healthcare resource utilization in real-world clinical practice.

Abbreviations

AD	Alzheimer's disease
AI	Artificial intelligence
ANTs	Advanced Normalization Tools
APOE	Apolipoprotein E
AUC	Area under the curve
Aβ	Amyloid-beta
CDR	Clinical Dementia Rating
CI	Confidence interval
CL	Centiloid
CSF	Cerebrospinal fluid
CT	Computed tomography
DAT	Dementia of the Alzheimer's type
FBB	18F-Florbetaben
FMM	18F-Flutemetamol
GAAIN	Global Alzheimer's Association Interactive Network
HU	Hounsfield units
K-ROAD	Korean Brain Aging Study for Early Diagnosis and Prediction of Alzheimer's Disease
MCI	Mild cognitive impairment
MRI	Magnetic resonance imaging

NPV	Negative predictive value
PET	Positron emission tomography
PPV	Positive predictive value
ROI	Region of interest
SD	Standard deviation
SIMOA	Single Molecule Array
SNSB	Seoul Neuropsychological Screening Battery
SUVR	Standardized uptake value ratio
p-Tau217	Phosphorylated tau 217

Supplementary Information

The online version contains supplementary material available at https://doi.org/10.1186/s13195-025-01870-z.

Supplementary Material 1: eNote 1. Summary of previously presented CT-based deep learning model. eFigure 1. Flow of participant selection. eFigure 2. The feature importance across cross-validation folds. eTable 1. Demographics of low-/intermediate-/high-risk group stratified by CT-based two-stage workflow and MRI-based two-stage workflow

Acknowledgements
The authors thank the participants and their families for their invaluable contributions. We also acknowledge the support of the K-ROAD study group for facilitating data collection. We also thank BeauBrain Healthcare for their contribution to amyloid PET image analysis and quantification.

Authors' contributions
SY and SP contributed equally as first authors. SY contributed to the conceptualization of the study, drafting of the manuscript, reviewing and editing the manuscript, data collection, and data curation. SP contributed to the conceptualization, data curation, and statistical analysis. KYL, HK, DS, HJ, MW, HZ, KB, FGO, NJA, SK, JY, MC, EK, HKim, DLN, and JPK contributed to data collection. SWS and KK contributed equally as corresponding authors and were responsible for conceptualization, study design, statistical analysis, manuscript review and editing, and overall supervision of the study.

Funding
This research was supported by a grant of the Korea Dementia Research Project through the Korea Dementia Research Center (KDRC), funded by the Ministry of Health & Welfare and the Ministry of Science and ICT, Republic of Korea (RS-2020-KH106434); by the Korea Health Technology R&D Project through the Korea Health Industry Development Institute (KHIDI), funded by the Ministry of Health & Welfare, Republic of Korea (RS-2025-02223212); by the National Research Foundation of Korea (NRF) grant funded by the Korea government (MSIT) (RS-2019-NR040057); by the Institute of Information & Communications Technology Planning & Evaluation (IITP) grant funded by the Korea government (MSIT) (RS-2021-II212068, Artificial Intelligence Innovation Hub); by the Future Medicine 20*30 Project of Samsung Medical Center (SMX1250081); and by the Korea National Institute of Health research project (2024-ER1003-01).
HZ is a Wallenberg Scholar and a Distinguished Professor at the Swedish Research Council supported by grants from the Swedish Research Council (#2023-00356, #2022-01018 and #2019-02397), the European Union's Horizon Europe research and innovation programme under grant agreement No 101053962, Swedish State Support for Clinical Research (#ALFGBG-71320), the Alzheimer Drug Discovery Foundation (ADDF), USA (#201809-2016862), the AD Strategic Fund and the Alzheimer's Association (#ADSF-21-831376-C, #ADSF-21-831381-C, #ADSF-21-831377-C, and #ADSF-24-1284328-C), the European Partnership on Metrology, co-financed from the European Union's Horizon Europe Research and Innovation Programme and by the Participating States (NEuroBioStand, #22HLT07), the Bluefield Project, Cure Alzheimer's Fund, the Olav Thon Foundation, the Erling-Persson Family Foundation, Familjen Rönströms Stiftelse, Stiftelsen för Gamla Tjänarinnor, Hjärnfonden, Sweden (#FO2022-0270), the European Union's Horizon 2020 research and innovation programme under the Marie Skłodowska-Curie grant agreement No 860197 (MIRIADE), the European Union Joint Programme – Neurodegenerative Disease Research (JPND2021-00694), the National Institute for Health and Care Research University College London Hospitals Biomedical Research Centre, the UK Dementia Research Institute at UCL (UKDRI-1003), and an anonymous donor.

Data availability
The datasets generated and analyzed during the current study are available from the corresponding author upon reasonable request.

Declarations

Ethics approval and consent to participate
This study was approved by the Institutional Review Board of Samsung Medical Center (No. 2021–02-135), and written informed consent was obtained from all participants and their caregivers in accordance with the Declaration of Helsinki.

Consent for publication
Not applicable.

Competing interests
SWS is co-founder of BeauBrain Healthcare Inc. SP, KL, and KK were employed by BeauBrain Healthcare Inc. HZ has served at scientific advisory boards and/or as a consultant for Abbvie, Acumen, Alector, Alzinova, ALZpath, Amylyx, Annexon, Apellis, Artery Therapeutics, AZTherapies, Cognito Therapeutics, CogRx, Denali, Eisai, Enigma, LabCorp, Merry Life, Nervgen, Novo Nordisk, Optoceutics, Passage Bio, Pinteon Therapeutics, Prothena, Quanterix, Red Abbey Labs, reMYND, Roche, Samumed, Siemens Healthineers, Triplet Therapeutics, and Wave, has given lectures sponsored by Alzecure, BioArctic, Biogen, Cellectricon, Fujirebio, Lilly, Novo Nordisk, Roche, and WebMD, and is a co-founder of Brain Biomarker Solutions in Gothenburg AB (BBS), which is a part of the GU Ventures Incubator Program (outside submitted work). KB has served as a consultant and on advisory boards for Abbvie, AC Immune, ALZPath, AriBio, BioArctic, Biogen, Eisai, Lilly, Moleac Pte. Ltd, Novartis, Ono Pharma, Prothena, Roche Diagnostics, and Siemens Healthineers; has served on data monitoring committees for Julius Clinical and Novartis; has delivered lectures, produced educational materials, and participated in educational programs for AC Immune, Biogen, Celdara Medical, Eisai and Roche Diagnostics; and is a co-founder of Brain Biomarker Solutions in Gothenburg AB (BBS), which is a part of the GU Ventures Incubator Program, outside the work presented in this paper.

Author details
[1]Department of Neurology, Samsung Medical Center, Sungkyunkwan University School of Medicine, 81 Irwon-ro, Gangnam-gu, Seoul 06351, Korea. [2]BeauBrain Healthcare, Inc., Hakdong-ro, Gangnam-gu, Seoul 06098, Korea. [3]Department of Neurology, Seoul National University Hospital, Seoul National University College of Medicine, Seoul, Jongno-Gu, Korea. [4]Department of Radiology and Biomedical Imaging, University of California, San Francisco, California, 1701 Divisadero St, San Francisco, CA 94115, USA. [5]Department of Psychiatry and Neurochemistry, Institute of Neuroscience and Physiology, The Sahlgrenska Academy at the University of Gothenburg, Gothenberg, Sweden. [6]Clinical Neurochemistry Laboratory, Sahlgrenska University Hospital, Mölndal, Sweden. [7]Department of Neurodegenerative Disease, UCL Institute of Neurology, Queen Square, London, UK. [8]UK Dementia Research Institute, UCL, London, UK. [9]Hong Kong Center for Neurodegenerative Diseases, Clear Water Bay, Hong Kong, China. [10]Wisconsin Alzheimer's Disease Research Center, School of Medicine and Public Health, University of Wisconsin, Madison, WI, USA. [11]Paris Brain Institute, ICM, Pitié-Salpêtrière Hospital, Sorbonne University, Paris, France. [12]Division of Life Sciences and Medicine, Department of Neurology, Institute on Aging and Brain Disorders, Neurodegenerative Disorder Research Center, University of Science and Technology of China and First Affiliated Hospital of USTC, Hefei, P. R. China. [13]King's College London, Institute of Psychiatry, Psychology and Neuroscience Maurice Wohl Institute Clinical Neuroscience Institute, London, UK. [14]NIHR Biomedical Research Centre for Mental Health and Biomedical Research Unit for Dementia at South London and Maudsley NHS Foundation, London, UK. [15]Centre for Age-Related Medicine, Stavanger University Hospital, Stavanger, Norway. [16]Department of Neurology, Korea University Guro Hospital, Korea University College of Medicine, Seoul, Korea. [17]Department of Neurology, KyungHee University College of Medicine, KyungHee University Hospital, Seoul, Korea. [18]Department of Neurology, Yonsei University College of Medicine, 50-1, Yonsei-Ro,

Seoul, Seodaemun-Gu 03722, Korea. [19]Department of Neurology, Yongin Severance Hospital, Yonsei University Health System, 363 Dongbaekjukjeon-daero, Giheung-gu, Yongin-si, Gyeonggi-do 16995, Korea. [20]Department of Neurology, Pusan National University Hospital, Pusan National University School of Medicine and Medical Research Institute, Busan, Korea. [21]Alzheimer's Disease Convergence Research Center, Samsung Medical Center, 81 Irwon-ro, Gangnam-gu, Seoul 06351, Korea. [22]Department of Health Sciences and Technology, SAIHST, Sungkyunkwan University, 115, Irwon-Ro, Gangnam-Gu, Seoul 16419, Korea. [23]Department of Digital Health, SAIHST, Sungkyunkwan University, 115, Irwon-Ro, Gangnam-Gu, Seoul 16419, Korea.

Received: 29 May 2025 Accepted: 11 September 2025
Published online: 28 October 2025

References

1. Scheltens P, Blennow K, Breteler MM, de Strooper B, Frisoni GB, Salloway S, et al. Alzheimer's disease. Lancet. 2016;388(10043):505–17.
2. Gorman AM. Neuronal cell death in neurodegenerative diseases: recurring themes around protein handling. J Cell Mol Med. 2008;12(6A):2263–80.
3. Wilson DM 3rd, Cookson MR, Van Den Bosch L, Zetterberg H, Holtzman DM, Dewachter I. Hallmarks of neurodegenerative diseases. Cell. 2023;186(4):693–714.
4. Budd Haeberlein S, Aisen PS, Barkhof F, Chalkias S, Chen T, Cohen S, et al. Two randomized phase 3 studies of aducanumab in early Alzheimer's disease. J Prev Alzheimers Dis. 2022;9(2):197–210.
5. Mintun MA, Lo AC, Duggan Evans C, Wessels AM, Ardayfio PA, Andersen SW, et al. Donanemab in early Alzheimer's disease. N Engl J Med. 2021;384(18):1691–704.
6. van Dyck CH, Sabbagh M, Cohen S. Lecanemab in early Alzheimer's disease. Reply. N Engl J Med. 2023;388(17):1631–2.
7. Lowe VJ, Mester CT, Lundt ES, Lee J, Ghatamaneni S, Algeciras-Schimnich A, et al. Amyloid PET detects the deposition of brain Abeta earlier than CSF fluid biomarkers. Alzheimers Dement. 2024;20(11):8097–112.
8. Mattsson N, Palmqvist S, Stomrud E, Vogel J, Hansson O. Staging beta-amyloid pathology with amyloid positron emission tomography. JAMA Neurol. 2019;76(11):1319–29.
9. Zammit MD, Tudorascu DL, Laymon CM, Hartley SL, Zaman SH, Ances BM, et al. PET measurement of longitudinal amyloid load identifies the earliest stages of amyloid-beta accumulation during Alzheimer's disease progression in Down syndrome. Neuroimage. 2021;228:117728.
10. Johnson KA, Fox NC, Sperling RA, Klunk WE. Brain imaging in Alzheimer disease. Cold Spring Harb Perspect Med. 2012;2(4):a006213.
11. Cicognola C, Brinkmalm G, Wahlgren J, Portelius E, Gobom J, Cullen NC, et al. Novel tau fragments in cerebrospinal fluid: relation to tangle pathology and cognitive decline in Alzheimer's disease. Acta Neuropathol. 2019;137(2):279–96.
12. Mattsson-Carlgren N, Andersson E, Janelidze S, Ossenkoppele R, Insel P, Strandberg O, et al. Abeta deposition is associated with increases in soluble and phosphorylated tau that precede a positive Tau PET in Alzheimer's disease. Sci Adv. 2020;6(16):eaaz2387.
13. Palmqvist S, Zetterberg H, Blennow K, Vestberg S, Andreasson U, Brooks DJ, et al. Accuracy of brain amyloid detection in clinical practice using cerebrospinal fluid beta-amyloid 42: a cross-validation study against amyloid positron emission tomography. JAMA Neurol. 2014;71(10):1282–9.
14. Duits FH, Martinez-Lage P, Paquet C, Engelborghs S, Lleo A, Hausner L, et al. Performance and complications of lumbar puncture in memory clinics: Results of the multicenter lumbar puncture feasibility study. Alzheimers Dement. 2016;12(2):154–63.
15. De Meyer S, Schaeverbeke JM, Luckett ES, Reinartz M, Blujdea ER, Cleynen I, et al. Plasma pTau181 and pTau217 predict asymptomatic amyloid accumulation equally well as amyloid PET. Brain Commun. 2024;6(4):fcae162.
16. Jack CR, Wiste HJ, Algeciras-Schimnich A, Figdore DJ, Schwarz CG, Lowe VJ, et al. Predicting amyloid PET and tau PET stages with plasma biomarkers. Brain. 2023;146(5):2029–44.
17. Mila-Aloma M, Ashton NJ, Shekari M, Salvado G, Ortiz-Romero P, Montoliu-Gaya L, et al. Plasma p-tau231 and p-tau217 as state markers of amyloid-beta pathology in preclinical Alzheimer's disease. Nat Med. 2022;28(9):1797–801.
18. Palmqvist S, Janelidze S, Quiroz YT, Zetterberg H, Lopera F, Stomrud E, et al. Discriminative accuracy of plasma phospho-tau217 for Alzheimer disease vs other neurodegenerative disorders. JAMA. 2020;324(8):772–81.
19. Masdeu JC, Pascual B. Neuroimaging of disorders leading to dementia. Curr Neurol Neurosci Rep. 2008;8(6):443–4.
20. Tartaglia MC, Rosen HJ, Miller BL. Neuroimaging in dementia. Neurotherapeutics. 2011;8(1):82–92.
21. Buckner RL, Snyder AZ, Shannon BJ, LaRossa G, Sachs R, Fotenos AF, et al. Molecular, structural, and functional characterization of Alzheimer's disease: evidence for a relationship between default activity, amyloid, and memory. J Neurosci. 2005;25(34):7709–17.
22. Chauveau L, Kuhn E, Palix C, Felisatti F, Ourry V, de La Sayette V, et al. Medial temporal lobe subregional atrophy in aging and Alzheimer's disease: a longitudinal study. Front Aging Neurosci. 2021;13:750154.
23. Jarholm JA, Bjornerud A, Dalaker TO, Akhavi MS, Kirsebom BE, Palhaugen L, et al. Medial Temporal lobe atrophy in predementia alzheimer's disease: a longitudinal multi-site study comparing staging and A/T/N in a clinical research cohort. J Alzheimers Dis. 2023;94(1):259–79.
24. Jobst KA, Smith AD, Barker CS, Wear A, King EM, Smith A, et al. Association of atrophy of the medial temporal lobe with reduced blood flow in the posterior parietotemporal cortex in patients with a clinical and pathological diagnosis of Alzheimer's disease. J Neurol Neurosurg Psychiatry. 1992;55(3):190–4.
25. Yim S, Park S, Lim K, Kwak K, Seo SW. Integrating MRI Volume and Plasma p-Tau217 for Amyloid Risk Stratification in Early Stage Alzheimer's Disease. Neurology. 2025;105(6):e213954.
26. Ghadimi M, Sapra A. Magnetic resonance imaging contraindications. Treasure Island (FL): StatPearls; 2025.
27. Hudson DM, Heales C, Meertens R. Review of claustrophobia incidence in MRI: a service evaluation of current rates across a multi-centre service. Radiography (Lond). 2022;28(3):780–7.
28. Metzner J, Domino KB. Risks of anesthesia or sedation outside the operating room: the role of the anesthesia care provider. Curr Opin Anaesthesiol. 2010;23(4):523–31.
29. Kim K. Computed tomography-based artificial intelligence for region-specific brain atrophy: differentiating the Alzheimer's continuum and frontotemporal dementia subtypes. IC-KDA, May 9 2025, Seoul, Korea. Abstract PE-32.
30. Lim KY, Park S, Na DL, Seo SW, Chun MY, Kwak K, et al. Quantifying brain atrophy using a CSF-focused segmentation approach. Dement Neurocogn Disord. 2025;24(2):115–25.
31. Jang H, Shin D, Kim Y, Kim KW, Lee J, Kim JP, et al. Korea-registries to overcome dementia and accelerate dementia research (K-ROAD): a cohort for dementia research and ethnic-specific insights. Dement Neurocogn Disord. 2024;23(4):212–23.
32. Petersen RC, Smith GE, Waring SC, Ivnik RJ, Tangalos EG, Kokmen E. Mild cognitive impairment: clinical characterization and outcome. Arch Neurol. 1999;56(3):303–8.
33. Albert MS, DeKosky ST, Dickson D, Dubois B, Feldman HH, Fox NC, et al. The diagnosis of mild cognitive impairment due to Alzheimer's disease: recommendations from the National Institute on Aging-Alzheimer's Association workgroups on diagnostic guidelines for Alzheimer's disease. Alzheimers Dement. 2011;7(3):270–9.
34. McKhann GM, Knopman DS, Chertkow H, Hyman BT, Jack CR Jr, Kawas CH, et al. The diagnosis of dementia due to Alzheimer's disease: recommendations from the National Institute on Aging-Alzheimer's Association workgroups on diagnostic guidelines for Alzheimer's disease. Alzheimers Dement. 2011;7(3):263–9.
35. Ryu HJ, Yang DW. The Seoul neuropsychological screening battery (SNSB) for comprehensive neuropsychological assessment. Dement Neurocogn Disord. 2023;22(1):1–15.
36. Fazekas F, Chawluk JB, Alavi A, Hurtig HI, Zimmerman RA. MR signal abnormalities at 1.5 T in Alzheimer's dementia and normal aging. AJR Am J Roentgenol. 1987;149(2):351–6.
37. Park S, Kim K, Yoon S, Kim S, Ahn J, Lim KY, et al. Establishing regional Abeta cutoffs and exploring subgroup prevalence across cognitive stages using BeauBrain Amylo((R)). Dement Neurocogn Disord. 2025;24(2):135–46.
38. Amadoru S, Doré V, McLean CA, Hinton F, Shepherd CE, Halliday GM, et al. Comparison of amyloid PET measured in Centiloid units with

neuropathological findings in Alzheimer's disease. Alzheimers Res Ther. 2020;12(1):22.
39. Bischof GN, Jacobs HIL. Subthreshold amyloid and its biological and clinical meaning: long way ahead. Neurology. 2019;93(2):72–9.
40. Royse SK, Minhas DS, Lopresti BJ, Murphy A, Ward T, Koeppe RA, et al. Validation of amyloid PET positivity thresholds in centiloids: a multisite PET study approach. Alzheimers Res Ther. 2021;13(1):99.
41. Schneider U, Pedroni E, Lomax A. The calibration of CT hounsfield units for radiotherapy treatment planning. Phys Med Biol. 1996;41(1):111–24.
42. Avants BB, Epstein CL, Grossman M, Gee JC. Symmetric diffeomorphic image registration with cross-correlation: evaluating automated labeling of elderly and neurodegenerative brain. Med Image Anal. 2008;12(1):26–41.
43. La Joie R, Perrotin A, Barré L, Hommet C, Mézenge F, Ibazizene M, et al. Region-specific hierarchy between atrophy, hypometabolism, and β-amyloid (Aβ) load in Alzheimer's disease dementia. J Neurosci. 2012;32(46):16265–73.
44. Yun J, Shin D, Lee EH, Kim JP, Ham H, Gu Y, et al. Temporal dynamics and biological variability of Alzheimer biomarkers. JAMA Neurol. 2025;82(4):384–96.
45. Yim S. Integrating MRI Volume and Plasma p-Tau217 for Amyloid Risk Stratification in Early Stage Alzheimer's Disease. IC-KDA, May 9 2025, Seoul, Korea. Abstract PE-240.
46. Jang H, Chun MY, Yun J, Kim JP, Kang SH, Weiner M, et al. Ethnic differences in the prevalence of amyloid positivity and cognitive trajectories. Alzheimers Dement. 2024;20(11):7556–66.

Publisher's Note